Environment International 193 (2024) 109127

Contents lists available at ScienceDirect

Environment International

journal homepage: www.elsevier.com/locate/envint

Full length article

Atmospheric monomethylmercury: Inferred sources constrained by observations and implications for human exposure

Peipei Wu [a,b], Zhengcheng Song [a,c], Peng Zhang [a], Shaojian Huang [a], Tengfei Yuan [a], Yanxu Zhang [d,*]

[a] School of Atmospheric Sciences, Nanjing University, Nanjing, Jiangsu 210023, China
[b] Scripps Institution of Oceanography, University of California, San Diego, La Jolla, CA 92093, USA
[c] Frontiers Science Center for Critical Earth Material Cycling, Nanjing University, Nanjing, Jiangsu 210023, China
[d] Department of Earth and Environmental Sciences, Tulane University, New Orleans, LA 70118, USA

ARTICLE INFO

Keywords:
Atmospheric monomethylmercury
Emissions
Human exposure
GEOS-Chem

ABSTRACT

Monomethylmercury (MMHg) is a potent neurotoxin that poses a threat to human health. MMHg cycles in all spheres of the Earth but the sources and fate of atmospheric MMHg are unclear. Here, we develop a global model for atmospheric MMHg, which integrates the presently available data and indicates the limitations of the current study. Constrained by the observations in the atmosphere, the global atmospheric MMHg from all sources is 1009 (205–2474 as an uncertainty range) Mg/yr, with the largest sources from the in-cloud methylation of divalent mercury (475 Mg/yr) and MMHg sea spray (395 Mg/yr). MMHg has a short lifetime of 1.9 days in the troposphere due to rapid photo-demethylation. Our model indicates a net loss of marine MMHg to the atmosphere and thus a detoxifying effect on MMHg contamination in marine fish. However, it suggests additional MMHg deposition to the land, particularly in densely populated coastal areas, introducing a new risk pathway that needs to be considered in mercury exposure assessment. The atmosphere plays a non-negligible role in the biogeochemical cycle and human health, which requires further study and consideration in implementing the global *Minamata Convention*.

1. Introduction

Monomethylmercury (MMHg) is a strong neurotoxin that can bioaccumulate and biomagnify in aquatic food webs, posing a significant threat to human health worldwide (Chen et al. 2008; Zhang et al. 2021). The aquatic MMHg is mainly produced by the microbe methylation of inorganic mercury (IHg) from the atmosphere, riverine runoff, and sediments (Amos et al. 2013; Kim et al. 2006; Lehnherr et al. 2011; Liu et al. 2021; Wang et al. 2022). Besides, direct atmospheric MMHg deposition is a potentially important source (Baya et al. 2015). However, previous studies mostly focus on the biogeochemical cycle of MMHg in the aquatic and terrestrial systems with few on the atmosphere, hindering our ability to accurately attribute the source of biota MMHg and mitigate the associated human exposure risks (Baya et al. 2015; Kim et al. 2017; Lavoie et al. 2013; Qin et al. 2016; Zhang et al., 2020b).

A variety of sources can contribute to the MMHg in the atmosphere: i) decomposition of dimethylmercury (DMHg) (Baya et al. 2015): DMHg is volatile and can be released from the ocean, municipal waste landfills, and wetlands (Baya et al. 2015; Lindberg et al. 2005; Wang et al. 2019); ii) direct releases of gaseous MMHg from the surface water, landfills, sludge-amended soil, and so on (Carpi et al. 1997; Lindberg et al. 2001; Mester and Sturgeon 2002); iii) the methylation of divalent mercury (Hg^{II}) in cloud water droplets with presence of acetic acid in the atmosphere (Gårdfeldt et al. 2003; Hammerschmidt et al. 2007). Field studies suggest that gaseous MMHg can bind to fine particles, with DMHg decomposition and MMHg volatilization as the largest source for the former (Zhang et al. 2019). Atmospheric MMHg is removed by photo decomposition in the aqueous phase and undergoes wet or dry deposition (Bittrich et al. 2011; Chen et al. 2018; Graydon et al. 2008; Zhang et al. 2012).

The available observations of atmospheric MMHg remain scarce, showing gaseous phase concentrations range from < 0.5–22 pg/m^3. The annual mean concentrations are 2.9 pg/m^3 in the Arctic and 7.4 pg/m^3 in a suburban area of Gothenburg, Sweden (Baya et al. 2015; Lee et al. 2003). There are much more measurements of MMHg concentrations in precipitation and wet deposition fluxes (Baya et al. 2015; Chen et al.

* Corresponding author.
E-mail address: yzhang127@tulane.edu (Y. Zhang).

https://doi.org/10.1016/j.envint.2024.109127
Received 22 August 2024; Received in revised form 12 October 2024; Accepted 4 November 2024
Available online 6 November 2024

2018; Huang et al. 2012; Lamborg et al. 1999; Qin et al. 2016; Weiss-Penzias et al. 2012; Xu et al. 2014; Zhang et al. 2012). These measurements are mostly located in East Asia and North America. The observed average MMHg concentrations in precipitation vary from 0.02 to 0.83 ng/L while the average wet deposition fluxes vary from 11 to 540 ng m^{-2} yr^{-1}.

This study develops a global transport and chemistry model for atmospheric MMHg by expanding the GEOS-Chem mercury (Hg) model. The model considers the sources, photolysis, and deposition of atmospheric MMHg, as well as the repartition of MMHg in different phases. The sources of atmospheric MMHg include the volatilization of DMHg from the ocean, landfills, and rice paddies and its decomposition, the spray of MMHg from the ocean surface, and the methylation of Hg^{II} in the aqueous phase. The spatial patterns of these sources are from the simulation of previous models or proxy data. We adopt a cost function to determine the most likely sources of MMHg in the atmosphere and their magnitudes are based on available observed data of MMHg concentrations in precipitation. The inferred sources are then used to drive the atmospheric MMHg model to simulate the transport and transformation of MMHg in the atmosphere. The marine MMHg spray and atmospheric MMHg deposition are also added to an ocean MMHg biomagnification model to evaluate the effects of air-sea exchange on MMHg levels in marine fish.

2. Methodology

2.1. GEOS-Chem model

The simulation of atmospheric MMHg is conducted in the global 3-D GEOS-Chem model (www.geos-chem.org; version 12.9.0). The model has a 2° latitude × 2.5° longitude horizontal resolution and 47 vertical layers extending to the mesosphere. In this study, we focus only on the MMHg in the troposphere, which is about 5–17 km in altitude depending on the locations in the model. Meteorological fields used to drive the model are from the NASA Modern-Era Retrospective Analysis for Research and Applications, version 2 (MERRA-2) system (Gelaro et al. 2017). GEOS-Chem model contains three Hg species: elemental mercury (Hg^0), divalent mercury (Hg^{II}), and Hg^{II} absorbed by particles ($Hg^{II}P$). The main Hg^{II} species include $Hg^{II}Cl_2$, $Hg^{II}Br_2$, $BrHg^{II}OH$, $Hg^{II}(OH)_2$, and so on. Excluding MMHg, anthropogenic Hg emissions are from Streets et al. (Streets et al. 2019) while other Hg emissions are from Horowitz et al. (Horowitz et al. 2017).

The photolysis of Hg^{II} and redox reactions of Hg^0 and Hg^{II} follow Shah et al., which suggest Br and OH are comparable contributors to global net oxidation of Hg^0 to Hg^{II} (Shah et al. 2021). The oxidant fields are the outputs of the full-chemistry simulation of GEOS-Chem (Wang et al. 2021). The model also includes the transformation of Hg^{II} and MMHg in aerosols and cloud droplets (Shah et al. 2021). DMHg can photodegrade and produce MMHg, which subsequently can degrade to Hg^{II} (Gårdfeldt et al. 2001; West et al. 2022). The photolysis of MMHg and DMHg follows that of organic particle Hg^{II}, which is scaled by multiplying the local NO_2 photolysis frequency by a scale factor. Previous estimates of demethylation rates of DMHg and MMHg in different waters vary from 2×10^{-4} to 0.42 d^{-1} and 0.2 to 0.54 d^{-1}, respectively (Lehnherr et al. 2011; West et al. 2022; West et al. 2020). The measurements of atmospheric MMHg photo decomposition rates are rare, with a few studies measuring atmospheric MMHg decomposition rates to be 0.19–19 d^{-1} in the liquid phase, reflecting the drastic variability of light environment (Bittrich et al. 2011; Gårdfeldt et al. 2001). We thus set the decomposition rates of DMHg and MMHg as 0.8 and 1.6 d^{-1}, respectively. The model also considers the dry and wet deposition of Hg species including the MMHg due to its solubility and affinity to particles (Shah et al. 2021; Zhang et al. 2019). Dry deposition velocities are determined by three types of resistances: aerodynamic, boundary, and surface resistance. Aerodynamic and boundary resistances are calculated from meteorological variables (e.g., windspeed and temperature), while surface resistance is largely based on the land use, surface characteristics (e.g., leaf area index), chemical properties of Hg species, and meteorological conditions. The partition between gaseous and particulate MMHg follows that between Hg^{II} and $Hg^{II}P$ as a function of local temperature and mass concentration of total particulate matter including sea salt (Amos et al. 2012). The mass accommodation coefficient α is adjusted to apply to a slower uptake of MMHg to aerosols than Hg^{II}. We run the model from 2012 to 2015 with the first three years as a spin-up and use the outputs of the last year for result analysis.

2.2. MMHg sources

Several sources of atmospheric MMHg are included in the model: volatilization and decomposition of DMHg, the spray of marine MMHg, and the methylation of Hg^{II} in the aqueous phase. According to previous studies, DMHg is released from the ocean, landfills, and wetlands such as rice paddies (Baya et al. 2015; Lindberg et al. 2005; Wang et al. 2019). The evasion fluxes of marine DMHg (F_{Docean}) are from existing outputs of an ocean mercury model based on the Massachusetts Institute of Technology general circulation model (MITgcm-Hg model) (Zhang et al., 2020a). Gaseous methylmercury (MeHg) concentrations are measured over local landfills or rice paddies but the global emission inventories are currently unavailable (Feng et al. 2004; Lindberg et al. 2005; Wang et al. 2019). The production of MeHg and CH_4 is associated with similar microbes in anaerobic environments so the emissions of CH_4 from solid waste landfills and agricultural soils are scaled as the emissions of DMHg from landfills (F_{Dldf}) and rice paddies (F_{Dagri}) (An et al. 2022; Evans et al. 2019; Gilmour et al. 2018). The CH_4 emissions are from the EDGARv7. GHG (Emissions Database for Global Atmospheric Research, global greenhouse gas) inventory (https://edgar.jrc.ec.europa.eu/).

MMHg has been detected in the ocean, landfills, and rice paddies, but only the direct emissions of MMHg from the ocean is considered in this study. Indeed, MMHg is much less volatile than DMHg, and we assume that marine MMHg in the open ocean is carried to the atmosphere by wind along with sea salt aerosols. The emissions of marine MMHg (F_{Mocean}) are scaled by MMHg concentrations in the surface ocean ($C_{MMHg,ocean}$) and emission fluxes of sea salt spray ($F_{seasalt}$). The MMHg concentrations are from the MITgcm-Hg model mentioned above (Zhang et al., 2020a). The sea salt spray fluxes depend on wind speed and sea surface temperature (Jaeglé et al. 2011):

$$F_{Mocean} = k_{Mocean} \times C_{MMHg,ocean} \times F_{seasalt} \times (1 - Frac_{seaice}) \quad (1)$$

$$F_{seasalt} = (0.329 + 0.0904T - 0.00717T^2 + 0.00027T^3) \times U_{10m}^{3.41} \quad (2)$$

where k_{Mocean} is a scaling factor adjusted by the observed MMHg concentrations in precipitation (elaborated below), $Frac_{seaice}$ is the fraction of sea ice in a model grid that ranges between 0 and 1, T is the sea surface temperature, and U_{10m} is the wind speed at 10 m height.

The relatively consistent ratio between MMHg and Hg^{II} in precipitation indicates that Hg^{II} is a substrate for MMHg (Hammerschmidt et al. 2007). The MMHg flux (F_{meth}) from the methylation of Hg^{II} is determined by the methylation rate (k_{meth}) and atmospheric Hg^{II} concentrations ($C_{Hg^{II}}$) (Hammerschmidt et al. 2007):

$$F_{meth} = k_{meth} \times C_{Hg^{II}} \quad (3)$$

The atmospheric Hg^{II} concentrations are simulated in the GEOS-Chem model.

2.3. Inferring emissions and production

The magnitudes of the above sources (i.e., F_{Docean}, F_{Dldf}, F_{Dagri}, F_{Mocean}, and F_{meth}) remain largely unknown. We keep the spatial pattern of these sources but their magnitudes are inferred by observations of MMHg in precipitation (Table S1). Observed MMHg concentrations are used rather than MMHg wet deposition because concentrations are more

robust and less sensitive to the variability of precipitation than deposition fluxes (Zhang and Jaeglé 2013). We run the model with individual sources to achieve the spatial pattern of atmospheric MMHg. A cost function (J) is used to represent the deviation between the modeled MMHg concentrations in precipitation and the observed ones (Fu et al. 2023):

$$J = \sum_{m} \left(\log_{10} C_{\text{model,m}} - \log_{10} C_{\text{obs,m}}\right)^2 \quad (4)$$

$$C_{\text{model,m}} = \sum_{n} S_{n,m} F_n \quad (5)$$

where m (=30) is the number of observed values, n (=5) is the number of sources, C is the MMHg concentrations in precipitation, S is the sensitivity of modeled MMHg concentrations in precipitation, and F is the emissions of each source. The inferred magnitudes of sources are obtained by minimizing J. We use the fminsearch function provided by MATLAB software to find the minimum of J. In fact, in addition to the observations, prior estimates and model uncertainty should also be included in the cost function (Brasseur and Jacob 2017). However, prior estimates are excluded here due to their unavailability and minimal weight in the cost function (Brahney et al. 2021). Model uncertainty is assessed through various scenarios (or an ensemble) that incorporate different assumptions about emissions and chemistry. More details on the simplification of the cost function and the consideration of model uncertainty are provided in supplementary materials.

The inferred individual emissions are then used to drive the atmospheric MMHg model one at a time. In this way, we can calculate the contributions of each source.

2.4. MMHg deposition to the ocean and its trophic transfer

We consider the MMHg air-sea exchange, i.e., atmospheric MMHg deposition to the ocean and direct marine spray, in an ocean MMHg biomagnification model (Wu and Zhang 2023). The model couples an ocean Hg model and ecological models to simulate the MMHg transfer from marine phytoplankton to fish on a global scale (Wu and Zhang 2023; Zhang et al., 2020a). The ocean Hg model simulates the biogeochemical cycle of marine Hg, including air-sea exchange, river discharge, redox reactions, sinking of particle mercury, methylation, and demethylation. The Hg^{II} deposition from air to the ocean and its methylation in the ocean are already considered in this model. As mentioned in the sections above, the ocean Hg model simulates the marine DMHg evasion. Also, this study adds the wet and dry deposition of atmospheric MMHg to the surface ocean in the ocean Hg model and removes the MMHg sea spray from the surface ocean. The model without MMHg air-sea exchange serves as a baseline model.

The coupled Darwin-Hg model simulates the passive uptake of MMHg by phytoplankton and the transfer of MMHg to zooplankton. Zooplankton can also obtain MMHg from seawater and they lose MMHg through excretion and death (Zhang et al., 2020a). The Darwin model has six categories of phytoplankton: two small phytoplankton (*Prochlorococcus* and *Synechococcus*), three large phytoplankton (diatoms, diazotrophs, and other large eukaryotic phytoplankton), and one intermediately sized phytoplankton (coccolithophores) (Dutkiewicz et al. 2009). There are also two categories of herbivorous zooplankton with different sizes and dietary preferences for phytoplankton.

The marine fish model (FEISTY) is coupled with the ocean Hg model to simulate the MMHg biomagnification in upper trophic levels of marine ecosystems. The fish model is based on the size and traits of fish and has five fish guilds: epipelagic fish, mesopelagic fish, large pelagic fish, mid-water predators, and demersal fish (van Denderen et al. 2021). The five fish guilds have different maximum body sizes, vertical distribution characteristics, and feeding strategies. Fish get MMHg from seawater and their food, including zooplankton, benthic production, and other fish with smaller body sizes. The same as zooplankton, fish lose MMHg through excretion and death. The mature fish spawn, and in this process, some of the MMHg in their bodies is transferred to the eggs.

2.5. Quality assurance/quality control

The models in this study, including atmospheric Hg model GEOS-Chem (Shah et al. 2021), marine Hg model MIT-gcm (Zhang et al., 2020a), marine ecosystem model Darwin and FEISTY (Dutkiewicz et al. 2009; van Denderen et al. 2021), are validated by observations and are widely used in related fields. The new species (i.e., MMHg and DMHg) added to GEOS-Chem may influence the simulation of existing species such as Hg^{II} but their modeled concentrations and spatial patterns are comparable with benchmarks. The emission inventory, EDGAR, integrates situ and remote sensing observations, conducts uncertainty analysis, and is verified by inverse models (Janssens-Maenhout et al. 2019).

The modeled concentrations of gaseous and particulate MMHg in the air, as well as MMHg in precipitation, are validated against available observed data (see further details of the comparison in Results and discussion section). These observed data, derived from field studies, have been peer-reviewed (Table S1).

The inferring of atmospheric MMHg sources is performed using fminsearch function in Matlab software, which has been employed in previous studies (Brahney et al. 2021; Fu et al. 2023). Here, a dataset of observed MMHg concentrations in precipitation serves as a constraint. We use "leave one out" strategy to assess the performance of the inferring process to this dataset. A total of 30 iterations, corresponding to the number of observed values, are performed. In each iteration, one observed value is dropped out. This will generate 30 sets of emissions and their distribution will be analyzed.

3. Results and discussion

3.1. Inferred emissions

The total atmospheric MMHg emitted or produced from all sources is 1009 Mg/yr (Fig. 1) with a 95 % confidence interval (CI) of 940–1139 Mg/yr around the minimum cost (Fig. 5c-d). The primary emissions (i.e., marine MMHg spray, decomposition of DMHg from the ocean, landfills, and rice paddies) are 534 (95 %CI: 469–655) Mg/yr, while the secondary production (Hg^{II} methylation) is 475 (95 %CI: 374–580) Mg/yr. The largest source is in-cloud Hg^{II} methylation (475 Mg/yr), followed by marine MMHg spray (395 Mg/yr), volatilization and decomposition of DMHg from the ocean (89 Mg/yr), landfills (43 Mg/yr), and rice paddies (7 Mg/yr) (Fig. 1). High fluxes of Hg^{II} methylation are over the southern hemisphere (Fig. 1c), where high concentrations of Hg^{II} from oxidation of Hg^0 and precipitation are favorable to the generation of MMHg (Dastoor and Larocque 2004; Shah et al. 2021). Hg^{II} methylation is a three-dimensional source and occurs mainly in the troposphere, with two peaks at 2 km and 11 km (Fig. S2), which is influenced by the vertical distribution of cloud fraction (i.e., aqueous phase) associated with convections (Xi et al. 2010).

The marine sources, including both direct marine MMHg emissions and volatilization and decomposition of marine DMHg, are relatively high in the eastern equatorial Pacific Ocean and high-latitude (latitude $> 60°$) oceans (Fig. 1b and 1d). The spatial patterns of these two sources are largely controlled by the distribution of ocean surface MeHg, with total emissions determined by the inferring process. Lower solar radiation and colder temperatures result in slower demethylation and thus higher MeHg concentrations in the high-latitude oceans. The atmospheric inorganic Hg deposition and enhanced microbial activity in the subsurface of the eastern equatorial Pacific Ocean favor the production of MeHg and its upwelling contributes to 17 % of the MeHg in the surface, resulting in the high MeHg concentrations in the surface ocean (Zhang et al., 2020a).

The two terrestrial sources, landfills and rice paddies contribute

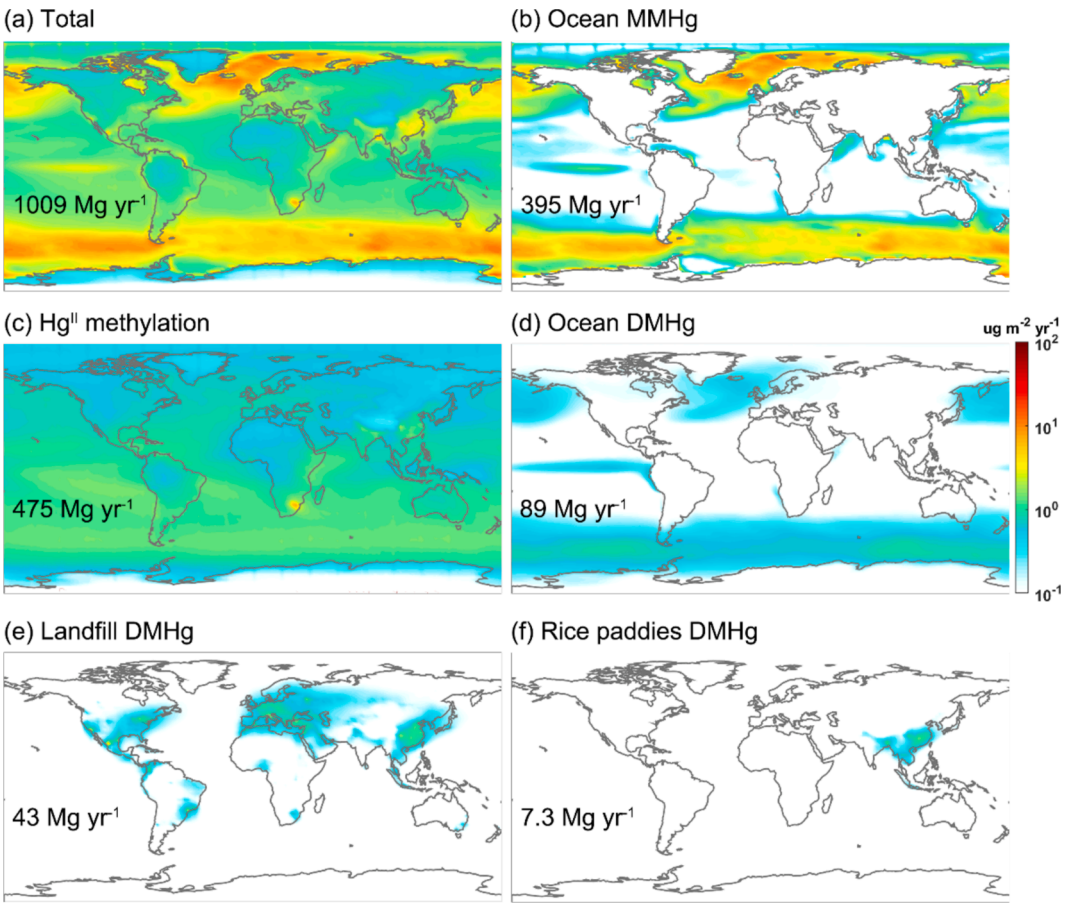

Fig. 1. Inferred MMHg emissions or production from various sources. (a) All sources; (b) MMHg from the ocean; (c) MMHg from the methylation of cloud and rain Hg^{II}; (d-f) MMHg from the volatilization and decomposition of DMHg from the ocean, landfills, and rice paddies, respectively. Note that fluxes in panels (c-f) are vertical integration in the troposphere.

relatively small amounts to the atmospheric MMHg (Fig. 1). The high emissions of MMHg from landfills are simulated in East Asia, Europe, and southern North America, associated with dense population and affluence (Fig. 1e) (Bogner and Matthews 2003). The emission fluxes from rice paddies are high in South and East Asia due to the concentrated rice cultivation in these areas (Fig. 1f) (Janssens-Maenhout et al. 2019). Although MMHg emissions from rice paddies account for less than 1 % of global total emissions, their contributions in some areas of South and East Asia are comparable to other major sources. The flooded soils of rice paddies provide an ideal environment for in situ methylation and are suggested to be sources of atmospheric MMHg in inland regions (Wang et al. 2019).

There are some prior estimates for atmospheric MMHg sources, such as Hg^{II} methylation rate and MMHg emissions from the volatilization and decomposition of ocean DMHg. The reported range of in-cloud Hg^{II} methylation rate in previous field and laboratory studies is $9.0 \times 10^{-7} - 5.4 \times 10^{-6}$ s^{-1} (Gårdfeldt et al. 2003; Hammerschmidt et al. 2007), and the rate inverted from the inferred production in this study is 1.8×10^{-6} s^{-1}, within the prior range. The emission of MMHg from the volatilization and decomposition of ocean DMHg (89 Mg/yr) is lower than that derived from the evasion flux of DMHg simulated by MITgcm (262 Mg/yr). The difference is attributed to the uncertainties of the constraint data and photodegradation rates of MeHg in this study (see Uncertainties section below), as well as the uncertainties of methylation transformation and air-sea exchange processes of MITgcm, but our estimate is within the uncertainty range of the MITgcm model (30–40 % for seawater MeHg concentrations but a factor of 2–3 for air-sea exchange fluxes) (Zhang et al., 2020a).

3.2. *MMHg in precipitation*

The inferred individual emission or production of MMHg discussed above is used to drive the atmospheric MMHg model one at a time. Fig. 2 shows the modeled spatial pattern of MMHg concentrations in precipitation and the contributions from each source. The model (0.15 ± 0.11 ng/L) generally reproduces the observed MMHg concentrations in precipitation ($n = 30$, 0.19 ± 0.19 ng/L), with slightly lower mean value and lower spatial variability than observations (Fig. 2a-b).

The two marine sources have a similar spatial pattern to the observed MMHg concentrations in precipitation (Fig. 1b, 1d, and 2b). Relatively high concentrations are measured in Hudson Bay (0.83 ng/L) and the Canadian Arctic Archipelago (0.4 ng/L), which are located in the high-latitude regions, with lower observed concentrations at middle latitudes ($30° < \text{latitude} < 60°$), and the lowest observed concentration of 0.02 ng/L over the equatorial Atlantic Ocean (Baya et al. 2015; Lamborg et al. 1999). Therefore, greater weight is allocated to these two sources when inferring the emissions. Indeed, direct marine MMHg emissions contribute to more than 70 % of the MMHg in precipitation in the high-latitude regions and mid-latitude oceans (Fig. 2c). Despite the similarity in the horizontal distribution of emissions (Fig. 1b and 1d), the estimated emission from the volatilization and decomposition of marine DMHg is much lower than direct marine MMHg emission. DMHg released from the ocean is transported throughout the atmosphere before it is decomposed into MMHg, so its contribution to the precipitation MMHg has different latitudinal distributions than sea MMHg spray (Fig. 2d). Similarly, Baya et al. show that atmospheric MMHg in the Arctic is from the ocean but the difference is that they suggest marine DMHg is the primary source based on the detected depletion of DMHg in

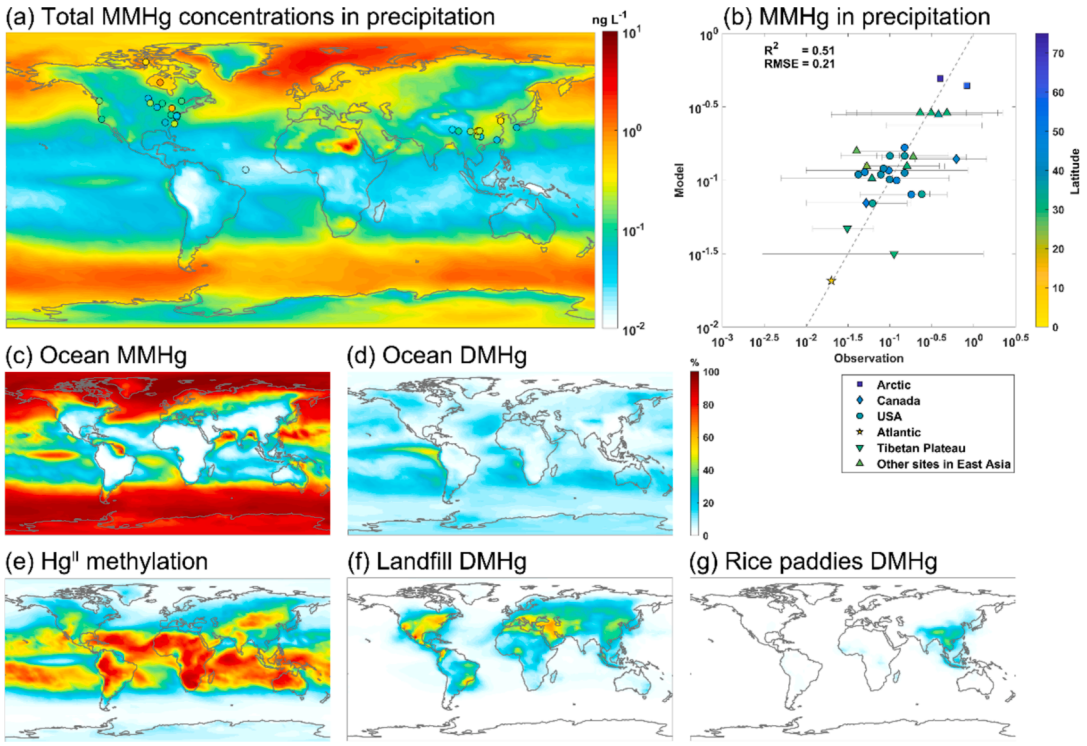

Fig. 2. Annual mean MMHg concentrations in precipitation. (a) MMHg concentrations in precipitation, (b) comparison with observations (Table S1), (c-g) the contribution of different sources: marine MMHg, Hg^{II} methylation, volatilization and decomposition of DMHg from the ocean, landfills, and rice paddies. In panel (a), the circles are observations from literature as listed in Table S1. In panel (b), the markers are the averages of observed values, the dashed line is the 1:1 line, the solid lines are the observed ranges, the shapes of the markers denote the regions, and the colors denote the latitude. R^2 and RMSE are calculated based on the logarithm of the concentrations.

the surface ocean (Baya et al. 2015). Both DMHg and MMHg can evade from the ocean and their actual evasion fluxes need more measurements to confirm (Mester and Sturgeon 2002; Soerensen et al. 2016).

The transport of MMHg from landfills is almost limited to land, contributing 30–50 % of the MMHg in southern North America, the areas around the Mediterranean Sea, and East Asia (Fig. 2f). MMHg from rice paddies is significantly concentrated in East Asia, where rice cultivation is widespread, accounting for 15–42 % of the total concentrations (Fig. 2g). The observed MMHg concentrations in precipitation are comparable in North America and East Asia while the MMHg emissions from landfills are also close in both regions, which is different from the distribution of MMHg emission from rice paddies that is concentrated in East Asia. As a result, the MMHg emission from landfills is weighted more heavily than emission from rice paddies in the inferring process, but both are much smaller than the marine sources and in-situ atmospheric methylation. The above four sources are from the ocean or land surface and they contribute 56 % of the simulated precipitation MMHg in Beijing, China, which is comparable to the contribution of similar sources to the atmospheric particulate MMHg (66.5 %) identified by a field study in this area, including DMHg decomposition, surface MMHg volatilization (waters, wetlands, sediments, or landfills), combustion, and marine sources (Zhang et al. 2019).

Direct in-cloud methylation of Hg^{II} plays an important role in the low-latitude (latitude $< 30°$) regions, with an average contribution of 54 % (Fig. 2e). Atmospheric Hg^{II} is widely distributed in the atmosphere and its methylation maintains atmospheric MMHg concentrations in areas of low marine or terrestrial sources. Indeed, the Hg^{II} methylation fluxes are high in the southern hemisphere but its contribution at middle and high latitudes is far outweighed by the ocean sources of MMHg. The observation at low latitudes remains scarce, but the model is consistent with the observation in the equatorial Atlantic Ocean, providing some constraint on this source (Fig. 2b).

3.3. Atmospheric MMHg budget

The mass of total MMHg (both gaseous and particulate MMHg) in the troposphere is 5.5 Mg (Fig. 3a). The largest removal pathway for atmospheric MMHg is through photodegradation (882 Mg/yr), followed by total deposition (201 Mg/yr). The majority of MMHg deposition is to the ocean (182 Mg/yr) and only 9 % is to the land (19 Mg/yr). The lifetime of atmospheric MMHg is 2.3 days against photodegradation and 10 days against total deposition. Overall, MMHg has a short lifetime of 1.9 days in the atmosphere, so relatively high emissions are needed to maintain the observed concentrations in precipitation. Compared with the existing Hg budget in the atmosphere, the MMHg mass accounts for only 0.14 % of the tropospheric inorganic Hg mass (4 Gg) (Shah et al. 2021). The total atmospheric MMHg emissions (excluding Hg^{II} methylation in the atmosphere) are 534 (469–655) Mg/yr, which is about 3.9–7.7 % of the total emissions for atmospheric Hg (8500–12000 Mg/yr) (Horowitz et al. 2017; Shah et al. 2021; Zhang et al. 2023). Indeed, atmospheric MMHg makes a much faster turn-over pool than atmospheric Hg^0 which has a lifetime of several months (Shah et al. 2021; Song et al. 2022).

3.4. Atmospheric MMHg concentrations and depositions

The spatial pattern of surface gaseous MMHg is largely determined by that of the sources (Fig. 3b and 1a). The short lifetime of MMHg prevents it from being transported a long distance in the atmosphere but is mostly distributed near sources. Indeed, the gaseous MMHg concentrations are higher in the high-latitude oceans, especially the Arctic Ocean connected to the Atlantic Ocean and the Southern Ocean adjacent to the Pacific Ocean. Surface particulate MMHg also has high concentrations at high latitudes. However, unlike the high concentrations of gaseous MMHg that occur over the ocean, the high concentrations of

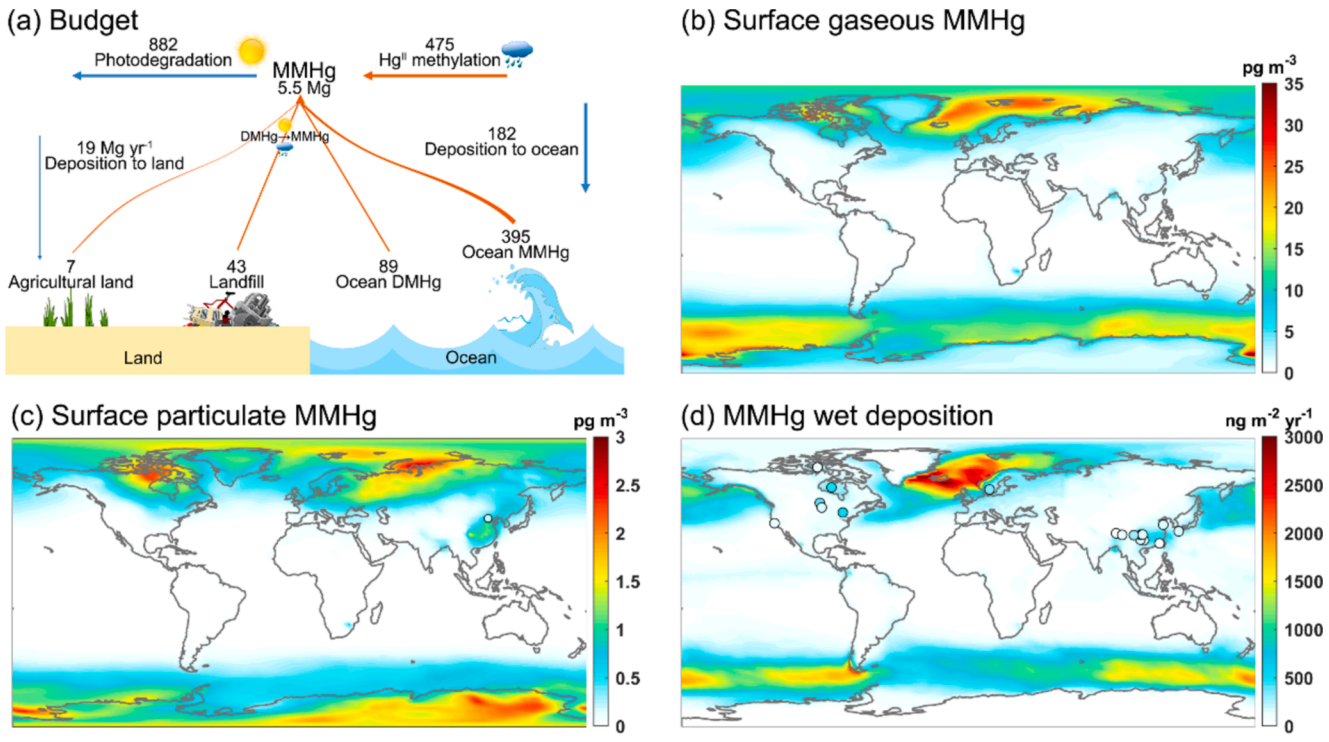

Fig. 3. (a) A global budget for atmospheric MMHg in the troposphere, (b) Modeled surface gaseous MMHg concentrations, (c) Modeled surface particulate MMHg concentrations, and (d) MMHg wet deposition fluxes. In panel (a), the sun denotes the photolysis and the cloud droplets denote the liquid-phase reactions. In panel (d), the circles are observations from literature as listed in Table S1.

particulate MMHg generally occur over the land (Fig. 3c). The modeled gaseous MMHg concentrations in the Arctic marine boundary layer are 2.7 ± 2.1 pg/m^3, close to the observations (2.9 ± 3.6 pg/m^3) (Baya et al. 2015). The modeled mean concentration is slightly lower (1.9 pg/m^3) in the suburban area of Gothenburg, Sweden, which is lower than the observation (7.4 pg/m^3) (Lee et al. 2003). Unlike in the Arctic, there are no observations of MMHg concentrations in precipitation in Europe to constrain the simulation here, resulting in large deviations between modeled and observed concentrations. The simulated annual mean concentration of particulate MMHg in Beijing, China is 0.72 pg/m^3, which is higher than the observed average concentration of 0.21 ± 0.17 pg/m^3 but within the observed range of < 0.01–1.33 pg/m^3 (Zhang et al. 2019). Overall, there is a lack of validation data for the modeling of gaseous and particulate MMHg and some uncertainties remain.

The wet deposition fluxes reflect the amount of precipitation and MMHg concentrations in the atmosphere. Similar to its concentrations in precipitation, the MMHg wet deposition is also much higher in the high latitudes than in the middle and low latitudes (Fig. 3d). The measurements of MMHg wet deposition are even more sparse and mostly located in the mid-latitude areas. Overall, the model (259 ± 169 ng m^{-2} yr^{-1}) reproduces the observed wet deposition fluxes (233 ± 174 ng m^{-2} yr^{-1}), but it slightly overestimates in East Asia and underestimates in North America. Over the Arctic Ocean, our modeled MMHg deposition is 14 Mg/yr, slightly higher than previous studies (2.6–10 Mg/yr) (Jonsson et al. 2022; Soerensen et al. 2016). Compared with MMHg concentrations in precipitation, the model deviation of the MMHg wet deposition fluxes from the measurements bears additional uncertainty from precipitation depths (Fig. 2a and 3d).

3.5. Uncertainties

Our results are subject to significant uncertainties that arise from the model parameters, proxy data, observational datasets, and inferring processes. For example, uncertainties can be introduced by the photodegradation rates of DMHg and MMHg. Furthermore, observed MMHg concentrations in precipitation as a constraint on emissions, proxy data for the spatial distribution of emissions, and atmospheric Hg^{II} and seawater MMHg/DMHg concentrations from previous models also contribute to the uncertainty in our emission estimates (Fig. 4). We discuss these aspects of uncertainty separately and compare their magnitudes.

The estimate of MMHg sources bears uncertainty due to potential inconsistencies in MMHg concentration measurements in precipitation. This means the estimate varies when different measurements are used as constraints. We adopt a "leave one out" strategy to estimate the uncertainty range of each source of MMHg: each data point is knocked out at a time in repeated inferring processes. The resulting ranges of the ensemble of MMHg from marine MMHg spray, Hg^{II} methylation, volatilization and decomposition of DMHg from the ocean, landfills, and rice paddies are 231–461, 318–682, 0–244, 23–50, and 0.3-11Mg/yr,

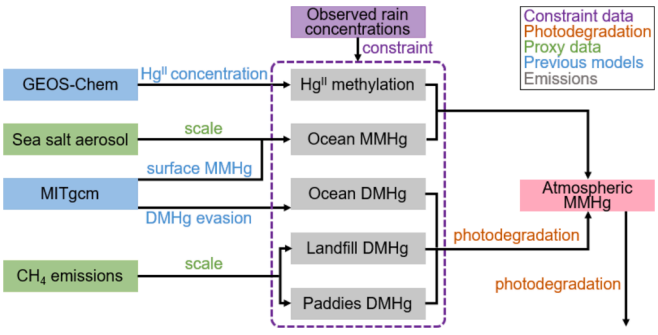

Fig. 4. A conceptual diagram of the model. The spatial patterns of emissions are scaled by proxy data or taken from previous models. The magnitudes of these emissions are constrained by the observed MMHg concentrations in precipitation. The uncertainties are from several factors: (i) the observed MMHg concentrations as a constraint on emissions, (ii) photodegradation rates of DMHg and MMHg, (iii) proxy data for emissions, and (iv) previous models as the foundations of this study.

respectively (Fig. 5a). The range of MMHg from total sources is consistently between 887 and 1170 Mg/yr, demonstrating good agreement across all observed data points.

Our estimate of MMHg emissions and production is closely associated with the decomposition rates of DMHg and MMHg. The former determines the MMHg generation rate from DMHg, and eventually the emissions from the ocean, landfill, and rice paddies, while the latter directly influences the atmospheric lifetime of MMHg and can impact our estimation of all sources. Based on the previously reported ranges of photodegradation rates of DMHg (2×10^{-4} to 0.42 d^{-1}) and MMHg (0.19–19 d^{-1}) in waters and atmospheric liquid environments (Bittrich et al. 2011; Gårdfeldt et al. 2001; Lehnherr et al. 2011; West et al. 2022; West et al. 2020), the photodegradation rates of MMHg and DMHg are perturbed by one order of magnitude, i.e., 0.13–1.3 and 0.51–5.1 d^{-1} for DMHg and MMHg, respectively, which results in a range of 436–2217 Mg/yr for total sources (Fig. 5b). As expected, when the photodegradation rate is elevated, higher emissions are required to maintain the observed MMHg concentrations in the atmosphere, especially the large elevations in the decomposition of marine DMHg and Hg^{II} methylation. Further higher photodegradation rate requires an unreasonably high volatilization flux of marine DMHg. Similarly, the simulated concentrations are not well fitted to the observed ones if the rate is too low.

Another source of uncertainty is the spatial proxy data we used for MMHg emissions (e.g., the CH_4 emission or sea salt spray flux). The microbes involved in Hg^{II} methylation and methanogenesis are not identical and sometimes the condition associated with MeHg production inhibits methanogenesis, resulting in differences in the spatial pattern of their emissions (Du et al. 2021; Wu et al. 2020). Sea salt aerosols are formed from the film and jet drops produced during the burst of bubbles and carried by wind from the ocean, during which the marine MMHg is possible to be carried to the atmosphere (Prather et al. 2013; Wang et al. 2017). However, the marine MMHg emissions scaled by sea salt spray ignore the direct volatilization of marine MMHg as it is more volatile when combined with halogens (e.g., CH_3HgCl) (Mester and Sturgeon 2002). The CH_4 emissions are from the EDGAR and the sea salt spray is affected by temperature and wind. To assess the uncertainties of these proxy data, we use CH_4 emissions from IIASA (International Institute for Applied Systems Analysis) and only consider the influence of wind speed on sea salt spray. We find that different proxy data do not significantly change the magnitude of emissions, with total emissions ranging from 1004 to 1107 Mg/yr (Fig. 5b).

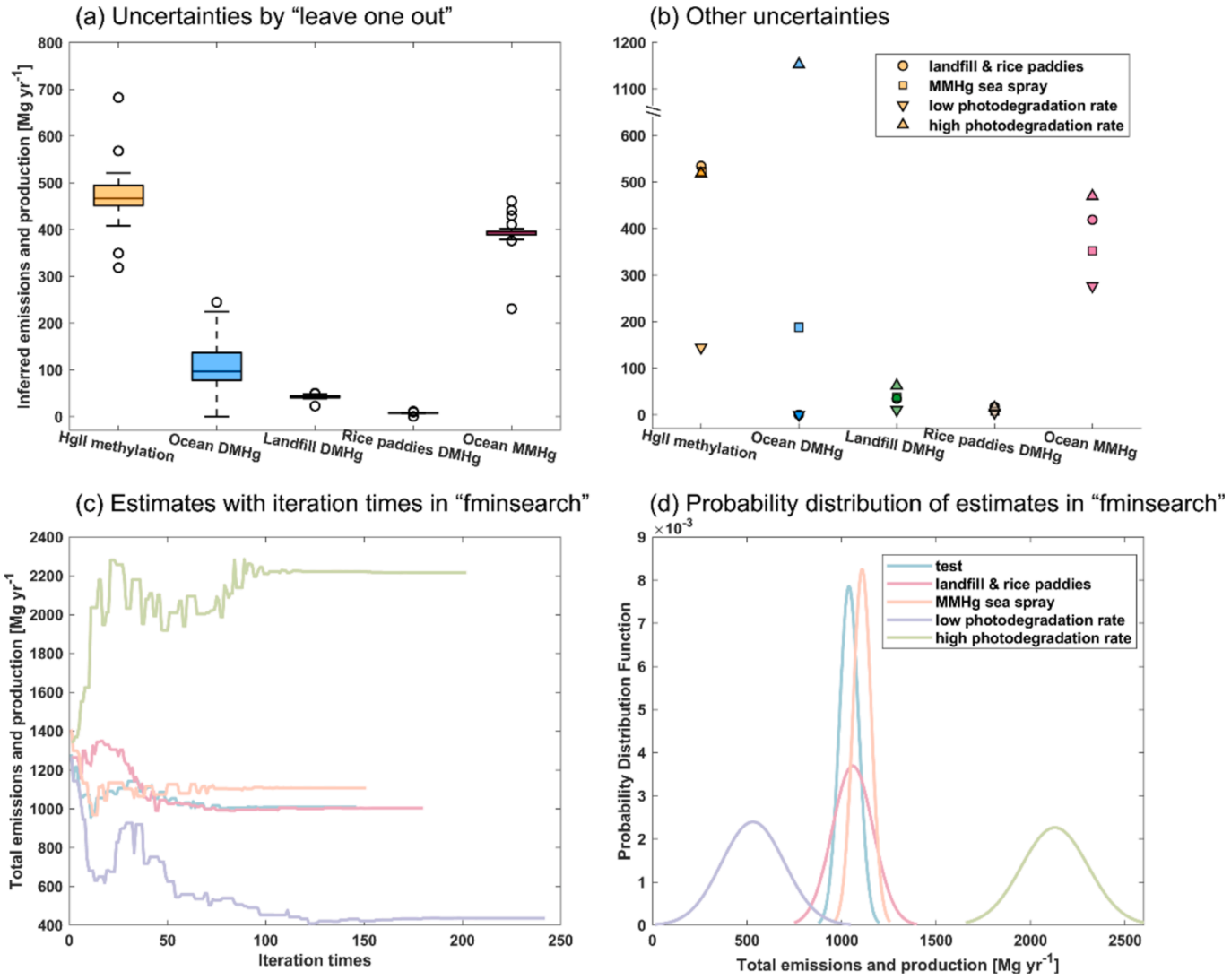

Fig. 5. Uncertainties of inferred emissions and production of MMHg from various sources. (a) Uncertainties by "leave-one-out" strategy; (b) uncertainties from proxy data for DMHg released from landfills and rice paddies, MMHg sea spray, and photodegradation rates; (c) total emissions and production of MMHg varying with iteration times in "fminsearch" processes; (d) probability distribution of total emissions and production estimated by "fminsearch" processes. "Test" is the scenario that used to analyze in the sections preceding the Uncertainties section.

In all the above scenarios, we provide emission estimates that minimize the deviation between the modeled and observed concentrations, i.e., the cost function. There is a range of estimates that vary with the number of iterations when using the "fminsearch" function to find the minimum cost. As shown in Fig. 5c, the emissions fluctuate around the final inferred value before reaching the minimum cost, and these values are also reasonable ranges for emission estimates. Estimates in different scenarios start from a similar value, with the medium estimate reaching the final value more quickly than the high- or low-end estimates and showing a narrower probability distribution (Fig. 5d). Considering the 95 % confidence intervals of those estimates near the minimum cost during the inferring process, the uncertainty range for the above scenarios widens slightly from 436–2217 to 205–2474 Mg/yr.

Finally, previous models used as foundations of this study, e.g., MITgcm-Hg and GEOS-Chem Hg model, bear some uncertainties. MITgcm-Hg model captures the spatial pattern of the observed MeHg in the surface ocean but slightly underestimates the concentrations (Zhang et al., 2020a). The simulated Hg^{II}, as a substrate for methylation, is from GEOS-Chem Hg model and is lower than the actual concentrations (Shah et al. 2021). The sources for atmospheric MMHg are constrained by the observed MMHg concentrations and the modeled MMHg concentrations in precipitation are consistent with the observed ones (Fig. 2b), indicating that the uncertainties of previous models do not largely propagate to this study.

Overall, the total uncertainty range of the inferred sources is 205–2474 Mg/yr, with the largest uncertainty arising from the photodegradation rates of DMHg and MMHg. The MMHg fluxes from decomposition of DMHg from landfills and rice paddies are also extrapolated significantly in this study because the evasion fluxes of DMHg from these areas are not reported in previous studies and their spatial patterns are scaled by CH_4 emissions. The other three sources are also rarely reported but the output of previous models, e.g., the modeled atmospheric Hg^{II} and seawater MMHg, can provide some constraints on the spatial patterns of Hg^{II} methylation, MMHg and DMHg released from the ocean although the previous models bear some uncertainties.

However, we find that Hg^{II} methylation and marine MMHg spray are always the primary sources while emissions from landfills and rice paddies are relatively small in all uncertainty scenarios (Fig. 5). Their spatial patterns are also relatively robust, due to their association with the underlying biogeochemical drivers. Indeed, our model is not a full-functioning predicting tool yet for the atmospheric MMHg levels because of the large uncertainty. It serves as a diagnostic tool to point out potentially important sources and processes, e.g., marine sources, Hg^{II} methylation, and photodegradation rates of MeHg, which require more direct observations and empirical evidence in future research.

3.6. Implications for human health

The global total MMHg deposition to the ocean is 182 Mg/yr, compensating for 46 % of the loss of ocean MMHg due to marine MMHg spray. The ocean has a net loss of 213 Mg of MMHg during the air-sea exchange (i.e., sea spray emissions − atmospheric deposition) per year, leading to a reduction in available MMHg for marine organisms. Compared with the simulation of the baseline model without MMHg air-sea exchange (Fig. S3), the simulated spatial pattern of MMHg concentrations in marine mature fish that are most relevant to marine fisheries and human exposure remains largely unchanged, with high concentrations in productive high-latitude regions and low in oligotrophic mid-latitude oceans (Fig. 6a) (Wu and Zhang 2023). However, the MMHg concentrations in fish are decreased by 4.0 % in the global ocean after considering the net loss of MMHg to the atmosphere (Fig. 6b), suggesting that the decrease of marine MMHg will be propagated to top predators in the marine ecosystems. The decreases are even higher in the high-latitude oceans where the modeled MMHg content in fish is relatively higher. For example, the maximum decrease is up to 34 % in the Southern Ocean and up to 69 % in the Arctic Ocean. This indicates a lower estimate of MMHg exposure from seafood consumption for the local populations than the modeling assessment without MMHg air-sea exchange.

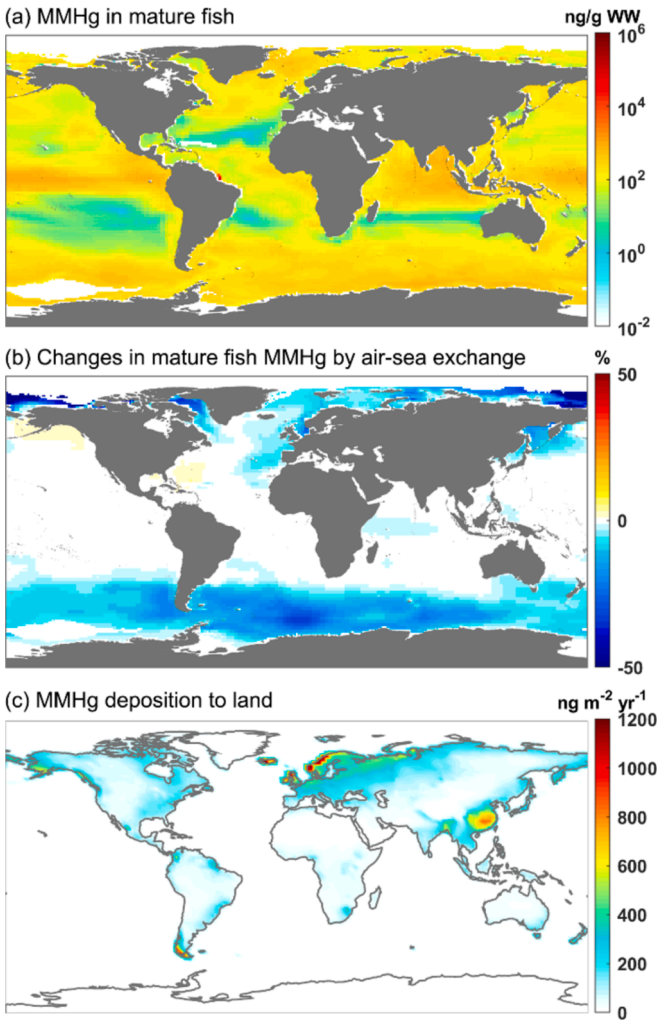

Fig. 6. Effects of atmospheric MMHg deposition on ocean and land. (a) The spatial pattern of MMHg concentrations in marine mature fish with MMHg air-sea exchange, (b) the relative changes in MMHg levels in mature fish by MMHg air-sea exchange, and (c) total atmospheric MMHg deposition to land.

Uncertainties in inferred emissions and model processes can propagate to the simulation of MMHg contamination in marine fish by affecting the marine MMHg spray and atmospheric MMHg deposition fluxes. A robust finding in all uncertainty scenarios shown in Fig. 5A-B is that the ocean is always a net source of atmospheric MMHg. The net loss of marine MMHg in these scenarios results in a 1.8–4.8 % reduction in the global average MMHg concentrations in marine mature fish (Fig. S4). The 95 % confidence interval of the reduction is narrow (3.7–4.1 %), due to the consistency in the observed data points discussed above. In addition, the maximum reduction in the Southern Ocean ranges between 19 % and 38 %, with a 95 % confidence interval of 32–34 %.

Previous studies also identify MMHg as an issue of concern in terrestrial ecosystems because of its close association with human exposure to rice and freshwater products (Driscoll et al. 2013; Liu et al. 2018; Liu et al. 2019; Xu et al. 2020). Our model indicates that the land is a net sink for atmospheric MMHg (19 Mg/yr), especially those populated coastal regions (Fig. 6c). The largest contributor to the MMHg deposition to land is marine MMHg spray (44 %), followed by Hg^{II} methylation (25 %), decomposition of DMHg from the landfills (20 %),

oceans (6.4 %), and rice paddies (4.6 %) (Fig. S5). The MMHg deposited to land increases the MMHg contaminations in rice paddies, rivers, and lakes that are related to human exposure. Indeed, this additional deposition is much higher than the global generation of MMHg in rice plants (3.5 Mg/yr) by a factor of 5 and the MMHg deposited to soils will be bioaccumulated by rice (Liu et al. 2019; Meng et al. 2011). Noticeably, the atmospheric MMHg deposition to East Asia with heavy rice cultivation is higher than to most other places on land, indicating potential higher health risks.

Our results reveal an atmospheric MMHg cycle that is largely overlooked in previous studies. With large sources from the ocean, the fast turnover of atmospheric MMHg provides a detoxification mechanism to reduce human exposure to marine MMHg. On the other hand, the net atmospheric transport of MMHg from the ocean to the land constitutes an additional risk to terrestrial ecosystems. It is necessary to consider that the atmospheric MMHg is severely understudied, and our conclusions derived from limited observations undergo large uncertainties. However, this study identifies the largest uncertainties and sheds light on future research directions. For example, more observations on photodegradation rates, which largely determine the fate of MMHg, or marine emissions and Hg^{II} methylation, which are potentially important sources, are needed. We thus call for more such studies as MMHg is the most toxic Hg chemical form that is most relevant to human health. The atmospheric MMHg cycle should be taken into full consideration for Hg pollution control and risk mitigation as required by the United Nations *Minamata Convention*.

CRediT authorship contribution statement

Peipei Wu: Writing – original draft, Visualization, Methodology, Investigation, Formal analysis, Data curation, Conceptualization. **Zhengcheng Song:** Methodology, Investigation, Funding acquisition. **Peng Zhang:** Investigation. **Shaojian Huang:** Investigation. **Tengfei Yuan:** Investigation. **Yanxu Zhang:** Writing – review & editing, Supervision, Project administration, Conceptualization.

Declaration of competing interest

The authors declare that they have no known competing financial interests or personal relationships that could have appeared to influence the work reported in this paper.

Acknowledgments

We acknowledge the financial support from the National Natural Science Foundation of China (NSFC) 42394094.

Appendix A. Supplementary data

Supplementary data to this article can be found online at https://doi.org/10.1016/j.envint.2024.109127.

Data availability

Data will be made available on request.

References

Amos, H.M., Jacob, D.J., Holmes, C.D., Fisher, J.A., Wang, Q., Yantosca, R.M., Corbitt, E. S., Galarneau, E., Rutter, A.P., Gustin, M.S., Steffen, A., Schauer, J.J., Graydon, J.A., Louis, V.L.S., Talbot, R.W., Edgerton, E.S., Zhang, Y., Sunderland, E.M., 2012. Gas-particle partitioning of atmospheric Hg(II) and its effect on global mercury deposition. Atmos. Chem. Phys. 12, 591–603.

Amos, H.M., Jacob, D.J., Streets, D.G., Sunderland, E.M., 2013. Legacy impacts of all-time anthropogenic emissions on the global mercury cycle. Global Biogeochem. Cycles 27, 410–421.

An, Y., Zhang, R., Yang, S., Wang, Y., Lei, Y., Peng, S., Song, L., 2022. Microbial mercury methylation potential in a large-scale municipal solid waste landfill, China. Waste Manage. 145, 102–111.

Baya, P.A., Gosselin, M., Lehnherr, I., St. Louis, V.L., Hintelmann, H., 2015. Determination of monomethylmercury and dimethylmercury in the Arctic marine boundary layer. Environ. Sci. Tech. 49, 223–232.

Bittrich, D.R., Rutter, A.P., Hall, B.D., Schauer, J.J., 2011. Photodecomposition of methylmercury in atmospheric waters. Aerosol Air Qual. Res. 11, 290–298.

Bogner, J.; Matthews, E. Global methane emissions from landfills: New methodology and annual estimates 1980–1996. Global Biogeochemical Cycles 2003;17: 2002GB001913.

Brahney, J., Mahowald, N., Prank, M., Cornwell, G., Klimont, Z., Matsui, H., Prather, K. A., 2021. Constraining the atmospheric limb of the plastic cycle. Proc. Natl. Acad. Sci. 118.

Brasseur, G.P., Jacob, D.J., 2017. Inverse Modeling for Atmospheric Chemistry. Cambridge University Press, Modeling of Atmospheric Chemistry.

Carpi, A., Lindberg, S.E., Prestbo, E.M., Bloom, N.S., 1997. Methyl mercury contamination and emission to the atmosphere from soil amended with municipal sewage sludge. J. Environ. Qual. 26, 1650–1655.

Chen, C., Amirbahman, A., Fisher, N., Harding, G., Lamborg, C., Nacci, D., Taylor, D., 2008. Methylmercury in marine ecosystems: Spatial patterns and processes of production, bioaccumulation, and biomagnification. Ecohealth 5, 399–408.

Chen, L., Li, Y., Liu, C., Guo, L., Wang, X., 2018. Wet deposition of mercury in Qingdao, a coastal urban city in China: Concentrations, fluxes, and influencing factors. Atmos. Environ. 174, 204–213.

Dastoor, A.P., Larocque, Y., 2004. Global circulation of atmospheric mercury: a modelling study. Atmos. Environ. 38, 147–161.

Driscoll, C.T., Mason, R.P., Chan, H.M., Jacob, D.J., Pirrone, N., 2013. Mercury as a global pollutant: Sources, pathways, and effects. Environ. Sci. Tech. 47, 4967–4983.

Du, H., Sun, T., Liu, Y., An, S., Xie, H., Wang, D., Igarashi, Y., Imanaka, T., Luo, F., Ma, M., 2021. Bacteria and archaea involved in anaerobic mercury methylation and methane oxidation in anaerobic sulfate–rich reactors. Chemosphere 274, 129773.

Dutkiewicz, S.; Follows, M.J.; Bragg, J.G. Modeling the coupling of ocean ecology and biogeochemistry. Global Biogeochemical Cycles 2009;23:2008GB003405.

Evans, P.N., Boyd, J.A., Leu, A.O., Woodcroft, B.J., Parks, D.H., Hugenholtz, P., Tyson, G. W., 2019. An evolving view of methane metabolism in the Archaea. Nat. Rev. Microbiol. 17, 219–232.

Feng, X., Tang, S., Li, Z., Wang, S., Liang, L., 2004. Landfill is an important atmospheric mercury emission source. Chin. Sci. Bull. 49, 2068–2072.

Fu, Y., Pang, Q., Suo Lang, Z.G., Wu, P., Wang, Y., Mao, M., Yuan, Z., Xu, X., Liu, K., Wang, X., Li, D., Zhang, Y., 2023. Modeling atmospheric microplastic cycle by GEOS-Chem: An optimized estimation by a global dataset suggests likely 50 times lower ocean emissions. One Earth 6, 705–714.

Gårdfeldt, K., Sommar, J., Strömberg, D., Feng, X., 2001. Oxidation of atomic mercury by hydroxyl radicals and photoinduced decomposition of methylmercury in the aqueous phase. Atmos. Environ. 35, 3039–3047.

Gårdfeldt, K., Munthe, J., Strömberg, D., Lindqvist, O., 2003. A kinetic study on the abiotic methylation of divalent mercury in the aqueous phase. Sci. Total Environ. 304, 127–136.

Gelaro, R.; McCarty, W.; Suárez, M.J.; Todling, R.; Molod, A.; Takacs, L.; Randles, C.A.; Darmenov, A.; Bosilovich, M.G.; Reichle, R.; Wargan, K.; Coy, L.; Cullather, R.; Draper, C.; Akella, S.; Buchard, V.; Conaty, A.; Silva, A.M.d.; Gu, W.; Kim, G.-K.; Koster, R.; Lucchesi, R.; Merkova, D.; Nielsen, J.E.; Partyka, G.; Pawson, S.; Putman, W.; Rienecker, M.; Schubert, S.D.; Sienkiewicz, M.; Zhao, B. The Modern-Era Retrospective Analysis for Research and Applications, Version 2 (MERRA-2). Journal of Climate 2017;30:5419– 5454.

Gilmour, C.C., Bullock, A.L., McBurney, A., Podar, M., Elias, D.A., 2018. Robust Mmercury methylation across diverse methanogenic *Archaea*. MBio 9, e02403–e2417.

Graydon, J.A., St. Louis, V.L., Hintelmann, H., Lindberg, S.E., Sandilands, K.A., Rudd, J. W.M., Kelly, C.A., Hall, B.D., Mowat, L.D., 2008. Long-term wet and dry deposition of total and methyl mercury in the remote boreal ecoregion of Canada. Environ. Sci. Tech. 42, 8345–8351.

Hammerschmidt, C.R., Lamborg, C.H., Fitzgerald, W.F., 2007. Aqueous phase methylation as a potential source of methylmercury in wet deposition. Atmos. Environ. 41, 1663–1668.

Horowitz, H.M., Jacob, D.J., Zhang, Y., Dibble, T.S., Slemr, F., Amos, H.M., Schmidt, J. A., Corbitt, E.S., Marais, E.A., Sunderland, E.M., 2017. A new mechanism for atmospheric mercury redox chemistry: Implications for the global mercury budget. Atmos. Chem. Phys. 17, 6353–6371.

Huang, J., Kang, S., Zhang, Q., Yan, H., Guo, J., Jenkins, M.G., Zhang, G., Wang, K., 2012. Wet deposition of mercury at a remote site in the Tibetan Plateau: Concentrations, speciation, and fluxes. Atmos. Environ. 62, 540–550.

Jaeglé, L., Quinn, P.K., Bates, T.S., Alexander, B., Lin, J.-T., 2011. Global distribution of sea salt aerosols: new constraints from in situ and remote sensing observations. Atmos. Chem. Phys. 11, 3137–3157.

Janssens-Maenhout, G., Crippa, M., Guizzardi, D., Muntean, M., Schaaf, E., Dentener, F., Bergamaschi, P., Pagliari, V., Olivier, J.G.J., Peters, J.A.H.W., van Aardenne, J.A., Monni, S., Doering, U., Petrescu, A.M.R., Solazzo, E., Oreggioni, G.D., 2019. EDGAR v4.3.2 Global Atlas of the three major greenhouse gas emissions for the period 1970–2012. Earth Syst. Sci. Data 11, 959–1002.

Jonsson, S., Mastromonaco, M.N., Wang, F., Bravo, A.G., Cairns, W.R.L., Chételat, J., Douglas, T.A., Lescord, G., Ukonmaanaho, L., Heimbürger-Boavida, L.-E., 2022. Arctic methylmercury cycling. Sci. Total Environ. 850, 157445.

Kim, E.-H., Mason, R.P., Porter, E.T., Soulen, H.L., 2006. The impact of resuspension on sediment mercury dynamics, and methylmercury production and fate: A mesocosm study. Mar. Chem. 102, 300–315.
Kim, H., Soerensen, A.L., Hur, J., Heimbürger, L.-E., Hahm, D., Rhee, T.S., Noh, S., Han, S., 2017. Methylmercury mass budgets and distribution characteristics in the Western Pacific Ocean. Environ. Sci. Tech. 51, 1186–1194.
Lamborg, C.H., Rolfhus, K.R., Fitzgerald, W.F., Kim, G., 1999. The atmospheric cycling and air–sea exchange of mercury species in the South and equatorial Atlantic Ocean. Deep Sea Research Part II: Topical Studies in Oceanography 46, 957–977.
Lavoie, R.A., Jardine, T.D., Chumchal, M.M., Kidd, K.A., Campbell, L.M., 2013. Biomagnification of mercury in aquatic food webs: A worldwide meta-analysis. Environ. Sci. Tech. 47, 13385–13394.
Lee, Y.H., Wängberg, I., Munthe, J., 2003. Sampling and analysis of gas-phase methylmercury in ambient air. Sci. Total Environ. 304, 107–113.
Lehnherr, I., St. Louis, V.L., Hintelmann, H., Kirk, J.L., 2011. Methylation of inorganic mercury in polar marine waters. Nat. Geosci. 4, 298–302.
Lindberg, S.E., Wallschläger, D., Prestbo, E.M., Bloom, N.S., Price, J., Reinhart, D., 2001. Methylated mercury species in municipal waste landfill gas sampled in Florida, USA. Atmos. Environ. 35, 4011–4015.
Lindberg, S.E., Southworth, G., Prestbo, E.M., Wallschläger, D., Bogle, M.A., Price, J., 2005. Gaseous methyl- and inorganic mercury in landfill gas from landfills in Florida, Minnesota, Delaware, and California. Atmos. Environ. 39, 249–258.
Liu, M., Chen, L., He, Y., Baumann, Z., Mason, R.P., Shen, H., Yu, C., Zhang, W., Zhang, Q., Wang, X., 2018. Impacts of farmed fish consumption and food trade on methylmercury exposure in China. Environ. Int. 120, 333–344.
Liu, M., Zhang, Q., Cheng, M., He, Y., Chen, L., Zhang, H., Cao, H., Shen, H., Zhang, W., Tao, S., Wang, X., 2019. Rice life cycle-based global mercury biotransport and human methylmercury exposure. Nat. Commun. 10, 5164.
Liu, M., Zhang, Q., Maavara, T., Liu, S., Wang, X., Raymond, P.A., 2021. Rivers as the largest source of mercury to coastal oceans worldwide. Nat. Geosci. 14, 672–677.
Meng, B., Feng, X., Qiu, G., Liang, P., Li, P., Chen, C., Shang, L., 2011. The process of methylmercury accumulation in rice (*Oryza sativa* L.). Environ. Sci. Tech. 45, 2711–2717.
Mester, Z., Sturgeon, R.E., 2002. Detection of volatile organometal chloride species in model atmosphere above seawater and sediment. Environ. Sci. Tech. 36, 1198–1201.
Prather, K.A., Bertram, T.H., Grassian, V.H., Deane, G.B., Stokes, M.D., DeMott, P.J., Aluwihare, L.I., Palenik, B.P., Azam, F., Seinfeld, J.H., Moffet, R.C., Molina, M.J., Cappa, C.D., Geiger, F.M., Roberts, G.C., Russell, L.M., Ault, A.P., Baltrusaitis, J., Collins, D.B., Corrigan, C.E., Cuadra-Rodriguez, L.A., Ebben, C.J., Forestieri, S.D., Guasco, T.L., Hersey, S.P., Kim, M.J., Lambert, W.F., Modini, R.L., Mui, W., Pedler, B.E., Ruppel, M.J., Ryder, O.S., Schoepp, N.G., Sullivan, R.C., Zhao, D., 2013. Bringing the ocean into the laboratory to probe the chemical complexity of sea spray aerosol. Proc. Natl. Acad. Sci. 110, 7550–7555.
Qin, C., Wang, Y., Peng, Y., Wang, D., 2016. Four-year record of mercury wet deposition in one typical industrial city in southwest China. Atmos. Environ. 142, 442–451.
Shah, V., Jacob, D.J., Thackray, C.P., Wang, X., Sunderland, E.M., Dibble, T.S., Saiz-Lopez, A., Černušák, I., Kellö, V., Castro, P.J., Wu, R., Wang, C., 2021. Improved mechanistic model of the atmospheric redox chemistry of mercury. Environ. Sci. Tech. 22, 14445–14456.
Soerensen, A.L., Jacob, D.J., Schartup, A.T., Fisher, J.A., Lehnherr, I., St. Louis, V.L., Heimbürger, L.-E., Sonke, J.E., Krabbenhoft, D.P., Sunderland, E.M., 2016. A mass budget for mercury and methylmercury in the Arctic Ocean. Global Biogeochem. Cycles 30, 560–575.
Song, Z., Sun, R., Zhang, Y., 2022. Modeling mercury isotopic fractionation in the atmosphere. Environ. Pollut. 307, 119588.
Streets, D.G., Horowitz, H.M., Lu, Z., Levin, L., Thackray, C.P., Sunderland, E.M., 2019. Global and regional trends in mercury emissions and concentrations, 2010–2015. Atmos. Environ. 201, 417–427.
van Denderen, P.D., Petrik, C.M., Stock, C.A., Andersen, K.H., 2021. Emergent global biogeography of marine fish food webs. Glob. Ecol. Biogeogr. 30, 1822–1834.
Wang, X., Deane, G.B., Moore, K.A., Ryder, O.S., Stokes, M.D., Beall, C.M., Collins, D.B., Santander, M.V., Burrows, S.M., Sultana, C.M., Prather, K.A., 2017. The role of jet and film drops in controlling the mixing state of submicron sea spray aerosol particles. Proc. Natl. Acad. Sci. 114, 6978–6983.
Wang, X., Jacob, D.J., Downs, W., Zhai, S., Zhu, L., Shah, V., Holmes, C.D., Sherwen, T., Alexander, B., Evans, M.J., Eastham, S.D., Neuman, J.A., Veres, P.R., Koenig, T.K., Volkamer, R., Huey, L.G., Bannan, T.J., Percival, C.J., Lee, B.H., Thornton, J.A., 2021. Global tropospheric halogen (Cl, Br, I) chemistry and its impact on oxidants. Atmos. Chem. Phys. 21, 13973–13996.
Wang, K., Liu, G., Cai, Y., 2022. Possible pathways for mercury methylation in oxic marine waters. Crit. Rev. Environ. Sci. Technol. 52, 3997–4015.
Wang, Z., Sun, T., Driscoll, C.T., Zhang, H., Zhang, X., 2019. Dimethylmercury in floodwaters of mercury contaminated rice paddies. Environ. Sci. Tech. 53, 9453–9461.
Weiss-Penzias, P.S.; Jr., C.O.; Acosta, R.P.; Heim, W.; Ryan, J.P.; Fernandez, D.; Jr., J.L. C.; Flegal, A.R. Total and monomethyl mercury in fog water from the central California coast. Geophysical Research Letters 2012;39:L03804.
West, J., Graham, A.M., Liem-Nguyen, V., Jonsson, S., 2020. Dimethylmercury degradation by dissolved sulfide and mackinawite. Environ. Sci. Tech. 54, 13731–13738.
West, J., Gindorf, S., Jonsson, S., 2022. Photochemical degradation of dimethylmercury in natural waters. Environ. Sci. Tech. 56, 5920–5928.
Wu, Q., Hu, H., Meng, B., Wang, B., Poulain, A.J., Zhang, H., Liu, J., Bravo, A.G., Bishop, K., Bertilsson, S., Feng, X., 2020. Methanogenesis is an important process in controlling MeHg concentration in rice paddy soils affected by mining activities. Environ. Sci. Tech. 54, 13517–13526.
Wu, P., Zhang, Y., 2023. Toward a global model of methylmercury biomagnification in marine food webs: Trophic dynamics and implications for human exposure. Environ. Sci. Tech. 57, 6563–6572.
Xi, B., Dong, X., Minnis, P., Khaiyer, M.M.A., 2010. 10 year climatology of cloud fraction and vertical distribution derived from both surface and GOES observations over the DOE ARM SPG site. JGR Atmospheres 115.
Xu, L., Chen, J., Yang, L., Yin, L., Yu, J., Qiu, T., Hong, Y., 2014. Characteristics of total and methyl mercury in wet deposition in a coastal city, Xiamen, China: Concentrations, fluxes and influencing factors on Hg distribution in precipitation. Atmos. Environ. 99, 10–16.
Xu, X., Han, J., Pang, J., Wang, X., Lin, Y., Wang, Y., Qiu, G., 2020. Methylmercury and inorganic mercury in Chinese commercial rice: Implications for overestimated human exposure and health risk. Environ. Pollut. 258, 113706.
Zhang, Y., Jaeglé, L., 2013. Decreases in mercury wet deposition over the United States during 2004–2010: Roles of domestic and global background emission reductions. Atmos. 4, 113–131.
Zhang, Z., Li, M., Li, Z., Xue, Z., Jiang, M., 2020. Unexpected high methylmercury contents related to soil organic carbon and its molecular composition in wetland soils of the Yarlung Tsangbo River. Tibet. Geoderma 377, 114607.
Zhang, X., Siddiqi, Z., Song, X., Mandiwana, K.L., Yousaf, M., Lu, J., 2012. Atmospheric dry and wet deposition of mercury in Toronto. Atmos. Environ. 50, 60–65.
Zhang, Y., Soerensen, A.L., Schartup, A.T., Sunderland, E.M., 2020. A global model for methylmercury formation and uptake at the base of marine food web. Global Biogeochem. Cycles.
Zhang, Y., Song, Z., Huang, S., Zhang, P., Peng, Y., Wu, P., Gu, J., Dutkiewicz, S., Zhang, H., Wu, S., Wang, F., Chen, L., Wang, S., Li, P., 2021. Global health effects of future atmospheric mercury emissions. Nat. Commun. 12, 3035.
Zhang, H., Wang, Z., Zhang, X., 2019. Methylmercury concentrations and potential sources in atmospheric fine particles in Beijing, China. Sci. Total Environ. 681, 183–190.
Zhang, Y., Zhang, P., Song, Z., Huang, S., Yuan, T., Wu, P., Shah, V., Liu, M., Chen, L., Wang, X., Zhou, J., Agnan, Y., 2023. An updated global mercury budget from a coupled atmosphere-land-ocean model: 40% more re-emissions buffer the effect of primary emission reductions. One Earth 6, 316–325.